Review of Scientific Instruments

High-speed laser speckle imaging to unravel picoliter drop-on-demand to substrate interaction

Cite as: Rev. Sci. Instrum. **92**, 083906 (2021); https://doi.org/10.1063/5.0011167
Submitted: 18 April 2020 . Accepted: 25 July 2021 . Published Online: 19 August 2021

R. Antonelli, R. Fokkink, N. Tomozeiu, J. Sprakel, T. E. Kodger, et al.

Review of Scientific Instruments ARTICLE scitation.org/journal/rsi

High-speed laser speckle imaging to unravel picoliter drop-on-demand to substrate interaction

Cite as: Rev. Sci. Instrum. 92, 083906 (2021); doi: 10.1063/5.0011167
Submitted: 18 April 2020 • Accepted: 25 July 2021 •
Published Online: 19 August 2021

R. Antonelli,[1] R. Fokkink,[1] N. Tomozeiu,[2] J. Sprakel,[1] and T. E. Kodger[1,a)]

AFFILIATIONS

[1] Physical Chemistry and Soft Matter, Wageningen University & Research, Stippeneng 4, 6708 WE Wageningen, The Netherlands

[2] Canon Production Printing, Sint Urbanusweg 43, 5914 CA Venlo, The Netherlands

[a)] **Author to whom correspondence should be addressed:** thomas.kodger@wur.nl

ABSTRACT

Understanding phenomena such as evaporation and imbibition of picoliter droplets into porous substrates is crucial in printing industry to achieve a higher printing quality and print speed. After printing, the residual pigment must remain fixed at the desired location on a substrate and be of a desired volume to yield a high resolution and vibrantly printed page that has become the expectation of modern printing technology. Current research entails not only chemical composition of the ink but also how this links to the dynamics and interactions that occur between the ink and the substrate at every stage of the printed spot formation, including evaporation, wetting, and imbibition. In this paper, we present an instrument that can print on-demand picoliter volume droplets of ink onto substrates and then immediately record on evolution of the resulting dynamics when these two materials interact. This high-speed laser speckle imaging (HS-LSI) technique has been developed to monitor nanometer displacement of the drying and imbibing ink droplet at a high frame rate, up to 20 000 Hz, given the short timescales of these interactions. We present the design of the instrument, discuss the related challenges and the theory underlying the LSI technique, specifically how photons non-evasively probe opaque objects in a multiple scattering regime, and show how this technique can unravel the dynamics of drying and imbibition. We will finish giving a validation on the instrument and an example of its usage.

I. INTRODUCTION

In printing industry, research efforts are currently focused on understanding evaporation and imbibition process of picoliter droplets.[1–7] In addition to new commercial inks and formulations, new machines and technologies are evolving. For example, UV-curable inks, pigment-based inks, a plethora of solvents and dyes, and more can now be printed on almost any kind of substrate.[8–11] Modern inkjet printheads can print thousands of very small picoliter droplets every second, reaching very high performances in resolution and color fidelity. However, errors still occur when new inks are developed or new substrates are tested.

There are a number of physical interactions that occur when a droplet hits a substrate: the ink contacts and wets, spreads onto, and imbibes into the substrate while evaporation occurs throughout this entire process, which lasts typically a few seconds. In most cases, swelling of the substrate also occurs as in the case of paper substrates,[12,13] dramatically altering each of these interactions. These concurrent phenomena make the description of the interaction quite challenging, both from a theoretical and practical point of view as a clear separation of timescales does not exist. Therefore particular conditions, in the general framework of liquid interacting with porous materials, remains unclear. The direct observation of the first evolution stages for picoliter droplets still remains quite challenging due to the micrometer dimensions and the speed of the process. For this reason, a large branch of research is focused on numerical simulation and studies on drop formation, involving complex fluid-dynamic physics,[14–17] also for the case of a mixture of two liquids only.

In this scenario, we present this High-Speed Laser Speckle Imaging (HS-LSI) instrument, which contains a set of moving printing inkjet nozzles traveling along a rail at the speed of 1 m/s, jetting a

series of 10 pl droplets above a target substrate, and illuminated by a laser immediately after the deposition. The ability of Laser Speckle Imaging (LSI) to non-destructively detect motions within the ink that occur at the nanometer length scale suits perfectly the target of study.[18,19] When impinging photons from a coherent light source, often a laser, illuminate an opaque material, they can undergo multiple scattering inside the sample. When they emerge in the direction of the camera, the subtle differences in path lengths leads to a characteristic interference or speckle pattern. If there is motion within the sample, caused by evaporation, diffusion, or another process, the speckle pattern fluctuates. The interpretation of these fluctuations reveals vital information about the dynamics of the turbid ink droplet, which would otherwise remain clouded. The use of laser light in HS-LSI facilitates high speed imaging necessary to probe the dynamics occurring at the short time and length scales associated with inkjet printing of picoliter droplets.

LSI is a procedure that until now is used mainly in medical imaging field, revealing, for example, under-skin or cerebral blood flow, and is a complementary technique to Doppler scans.[18,20–22] The theory that stands behind LSI, which was developed starting from the 1990s, is the evolution of the Dynamic Light Scattering (DLS) and is known as Diffusing Wave Spectroscopy (DWS).[23] In DWS, only one speckle at a time can be addressed to evaluate the system dynamics. With LSI, a Region Of Interest (ROI) is probed: the area depends on the camera sensor and magnification used; in addition, the speckle size, which depends on the optical components, plays a crucial role in LSI measurements. All these criteria had been considered to optimize the instrument performances.

In recent years, LSI technique has been developed outside of the medical field, and it has been applied in a variety of scenarios.[24–26] It has been used to study crack patterns in drying films of 50–200 μm thickness, droplets, and paints.[27,28] Here, the authors were able to generate quantitative results on dynamics and timescales of these systems. LSI has also been used in the field of painting renovation to study the response of oil paintings when exposed to organic solvents for varnish removal or to water for the removal of surface dirt.[29] The depth of the studied region ranged from 7 to 21 μm, which is comparable to the length scale of inkjet printed droplets studied here. Crucially, in this case, LSI is capable to provide quantitative results. In other works, LSI has been applied, yielding results in line with simulations to study fractures in soft solids and dynamics of thin ($\mathcal{O} \sim 10$ μm) films of turbid media.[25,30] The ability of LSI to be adapted in such different fields is impressive.

In this paper, we show how we combined this scientific technique, LSI (capable of capturing very fast motion with a very high magnification), with a printing technology to unravel the scope and dynamics of drying picoliter droplets. In Sec. II, we present the instrument: the moving cartridge and the power of the laser light are driven by home-made MATLAB programs, while the cartridge heater/thermometer and printing regulation are driven through an Arduino Mega board. Then, we present how printing droplets are triggered by wave signals driven by an external wave generator, activated by position sensors. All the components and processes will be examined to ensure the reproducibility of the setup and the measurements. After, we briefly explain LSI theory and show its suitability for printing measurements; we show two possible approaches, autocorrelation functions and fast Fourier transform method, to interpret the collected data. Finally, we finish by giving one example of its usage.

II. THE INSTRUMENT

A schematic rendering of the instrument is presented in Fig. 1. The instrument is divided into four sections: (a) mechanical parts; (b) electrical components, i.e., power and signal lines; (c) laser elements; and (d) camera and optics. The central part of the instrument consists of a 595 mm length motorized rail (Zaber Technologies linear axis X-BLQ0595-E01-PTB2) with a moving stage, which is connected through an aluminum support to an inkjet printing device (Fujifilm Dimatix DMC-11610), consisting of a piezo-driven jetting device with an integrated reservoir and heater: a total of 16 printing nozzles, at the distance of 256 μm between each other, disposed in a row. Each nozzle can produce a series of 10 pl volume droplets on demand, triggered with a pulse sequence, which will be described later. The printhead and support (weight = 1.5 kg) rest on the stage, moving together with an acceleration of 2000 mm/s^2, at a maximum velocity of 1200 mm/s in both directions. The communication to the

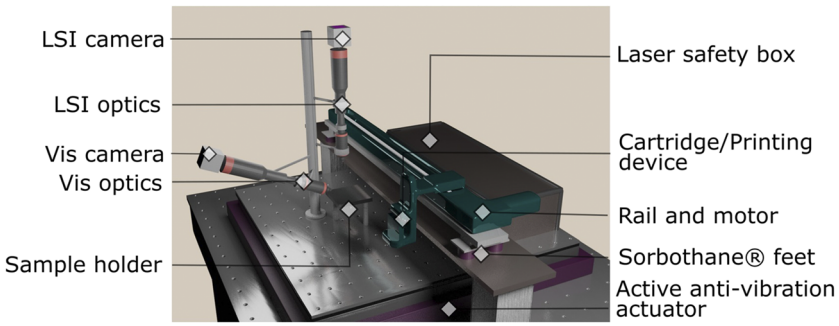

FIG. 1. Schematic of the instrument: An open inkjet printing device with a cartridge/printing device head driven on a rail and motor (green colors). Running at a velocity of ~1 m/s, from right to left in the schematic, and while passing over the sample holder, the printing head is triggered to eject a series of picoliter droplets onto the substrate sitting on the sample holder. The printed drop is immediately illuminated by coherent laser light from the laser safety box and steered with mirrors, not shown in the schematic. Photons scatter within the sample and are collected by LSI optics and a camera. An active anti-vibration actuator and Sorbothane feet (purple colors) are fundamental to isolate the sample holder and LSI optics from vibrations arising from the movement of the rail and motor. A VIS camera and optics capture images with visible white light from an oblique angle.

PC occurs via a Universal Serial Bus (USB) connection, accepting movement commands and the device settings sent by the operator through home-made MATLAB scripts. The rail contains a rotary quadrature encoder, which can detect the position of the stage within an accuracy of 10 μm.

As LSI measurements can detect displacements that happens at the nanometer length scale,[31] a crucial aspect in the design of the instrument is to avoid vibrations arising from the movement of the rail to reach the sample holder and the optical components. Consider that in ~60 cm, the printhead and its support travel from a rest state to a speed of 1200 mm/s and then stop at the end of the rail. These components are placed on a home-designed aluminum support, which was previously treated to avoid undesirable scattering from the laser, and with a pair of pillars, the overall design is placed on a vibrationally isolated optical table. A first vibration dumping is actuated by Sorbothane feet [Sorbothane® Male Vibration Stud Bumper Mount—M6—21.6 mm (H)—44.5 mm (Dia) 70 Durometer] placed between the rail and the supporting aluminum plate. The laser, the sample holder, the optics, and the camera are all placed on a smaller optical breadboard, which is vibrationally disconnected from the moving stage by an active vibration isolation device (Accurion i4) that acts as a further, and crucial, vibration dump (see Fig. 1). This particular device actively dampens 99% of the frequencies between 1 and 200 Hz and passively dumps higher frequencies. Since in this study we do not take into account frequency lower than 1 Hz, this kind of insulator is ideally suited.

Standing on two posts, just below the printing point of the cartridge, on the small optic breadboard is a sample holder: a manual moving stage (Thorlabs XYT1/M) that can travel 13 mm both in X and Y direction. This particular stage is very useful for two reasons. First, it has a 20 mm round hole in the center, which allows for the possibility of performing measurements in transmission, made by placing the optics and camera beneath the void space. Second, the stage may be moved laterally with two translational micrometers knobs. This application is useful for small samples such that it is practical to print on the desired area of the substrate. Moreover, a line of printed droplets, for each measurement, span a width of not more than 200 μm: moving the stage by 500 μm allows new measurement to be performed on a fresh area of the same substrate.

To be able to print the desired droplets, the printing device is connected to a wave generator (Aim-TTi International, model TGA 1240). Each printing pulse, which allows for the production of a single drop from the nozzle, lasts for about 35 μs, resulting in challenging synchronization between the movement of the stage, traveling at a velocity of ~1 m/s, and the firing pulse. Consider also that achieving high frame rates requires that the field of view of the camera be reduced to 150 μm or ~300 pixels in x and y directions. The type of connection from the rail motor to the computer, which is a standard USB cable, and the computational time that is required to process the positional information inhibit the instantaneous command communication with the printing device. This means that while the stage is moving, it is impossible to accurately read out its position and trigger the printing command at the same time. For this reason, a movement sensor (Optek/TT Electronics model OPB-960-T11) was installed on the rail as a starter for the wave generator to begin firing printing pulses. Even though the response of this sensor is 70 ns and directly triggers the wave generator with a coaxial cable, the imprecision on a single printed drop with a radius of about 30 μm is large enough such that the drops can be printed partially or completely out of the 150 μm reduced field of view. Therefore, many drops are printed during a single pass of the printing cartridge, and only if a drop is fully within the imaging field of view is the process considered successful.

The electrical connections of the system are presented in Fig. 2. Dashed lines represent power cables, while continuous lines represent signals and data cables. Note the use of different power supplies: 220 V AC for the PC, camera, moving stage, and laser; 40 V DC for the CMOS transistor; and 20 V DC for the movement sensor and heater. A voltage regulator, with a range of 0–20 V, is used to control the amount of power directed to the printhead heater for the control of the temperature of the ink and can be adjusted from room temperature to 120 °C. Coaxial cables are used to trigger the wave generator from the movement sensor. Standard coaxial cables are adopted also to carry the printing pulses from the wave generator to a voltage amplifier (FLF Electronics, model F20A) and then to a precision CMOS analog switch (Vishay Siliconix DG 417), which allows for opening or closing the signal printing path. If the channel is open, the signal can travel from the switch to the printhead with copper wires to produce the desired droplets. Just before entering the printing device, the line is split into two parts: one part is directed to the printhead, while the other is directed to an oscilloscope (Tektronics, TBS1022). Using this device, the incoming signal can be effectively controlled to have the shape and power required to activate the piezoelectrics in the printhead. These piezoelectrics are the active part of the printhead and have the ability to expand or compress the ink chamber. To produce a droplet, the ink chamber, situated just above the nozzle, must experience an expansion at first, which allows the ink to flow into the chamber itself, followed by a rapid contraction, pressing the ink through the nozzle. Each of the 16 nozzles is allowed to print by connecting or disconnecting any of the 16 cables that transfers the signal to the printhead in a nozzle relay (NR in Fig. 2).

These printing functional commands, excluding the camera control, are executed through a home-made MATLAB GUI. This program sends commands to an Arduino Mega board, which opens and closes the printing channel using the CMOS analog switch: this board sends a square wave of 5 V when the channel has to be open

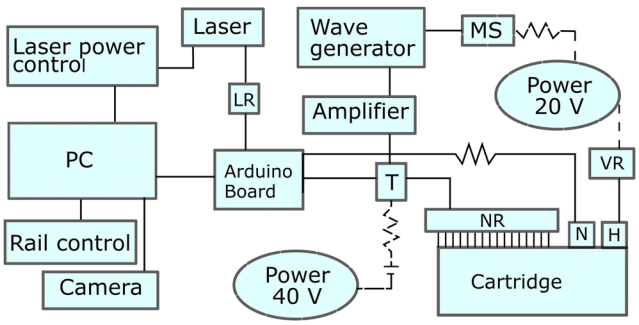

FIG. 2. Schematic of electrical components: Dashed line for power lines and solid lines for signal lines. LR = laser relay, MS = movement sensor, T = CMOS transistor, NR = nozzle relay, VR = voltage regulator, N = NTC, and H = heater.

and is set to 0 V if the channel is closed. Additionally, it controls the on\off switching of the laser light. This last operation is carried out using a mechanical relay. As for the analog switch, a square wave of 5 V controls the relay. Since the laser power is very sensitive to power fluctuation, a mechanical relay instead of a transistor is used to avoid any instability and delays caused by capacitors and analogical components present inside a transistor. The last function of the Arduino board is to read out the temperature of the printhead, achieved using a Negative Temperature Coefficient thermoresistor (NTC) present in the printhead by fabrication. These electronic components are able to decrease their internal electrical resistance when the temperature increases. The Arduino board reads out the amount of power that passes through this component, obtaining the temperature. A further application of the MATLAB GUI is to control the speed, acceleration, and position of the linear axis using a USB connection from the PC to the motorized stage and the amount of laser power directed to the specimen.

Laser power is actuated by a motorized precision rotation stage, mounted with a half wave plate (Fig. 3), bundled with a DC servo motor driver (Thorlabs KPRM1E). The communication is actuated from the PC to the servo motor using the ATP Thorlabs software, which is integrated in the MATLAB GUI, and from here to the rotational stage. ATP software controls the angular position of the rotational stage and thus the intensity of the exiting laser beam. The laser source, which is placed on a custom-made cooling plate to avoid the over-heating of the source, has a constant output of 1 W, power that is too large for the majority of the test due to both burning paper and ink. Laser power is controlled by diverting a portion of the laser into a beam dump using a polarizing beam splitting cube. The light emerging from the source is linearly polarized, and using a half wave plate, it is possible to rotate the polarization depending on the rotational angle it is placed with respect to the emitting source. This means that depending on the half-wave plate rotational angle, which is controlled by the operator, part of the incident light will pass through the beam splitting cube, while the rest will be reflected toward the beam dump, as shown in Fig. 3. Knowing the dependency of the amount of the linearly polarized light which passes through varying the angle on the rotational stage, the laser power impinging on the specimen is precisely controlled without the power supply current to the laser being constantly changed. The result is a stable, tunable, laser power onto the specimen. For safety reasons, these components are enclosed in a laser proof box.

With this design, the incident light impinging the sample is linearly polarized. This property is extremely important in LSI measurements to avoid singly scattered photons: only photons that have traveled more than a certain distance inside the sample, the mean free path l^*, should be collected by the camera.[27,30,32–35] We define l^* as the distance after which the photon directionality is completely randomized. To collect only these photos, a linear polarizer acting as an analyzer is placed in the optical path before the camera. The role of this component is to block the photons that have the same polarization of the incident light, effectively removing photons that have traveled less than $\mathcal{O} \sim 3l^*$.[36] The analyzer is mounted on a rotational stage. This configuration allows us to rotate it in a position of minimum incoming light coming from the sample.

Finally, in the instrument design, other optical components from the specimen to the camera sensor are necessary to achieve a high magnification to visualize ink droplets that have $r \sim \langle 30\ \mu\text{m} \rangle$. The working distance between the sample and the objective must be sufficient to allow the cartridge to pass underneath; this is achieved by an objective (Thorlabs MVL12X12Z) with a further magnify lens (Thorlabs MVL12X05L) installed. These two components allow for a working distance of 165 mm, allowing the cartridge, with a height of 110 mm, to move undisturbed between the sample holder and the optical components. After the lens, the analyzer

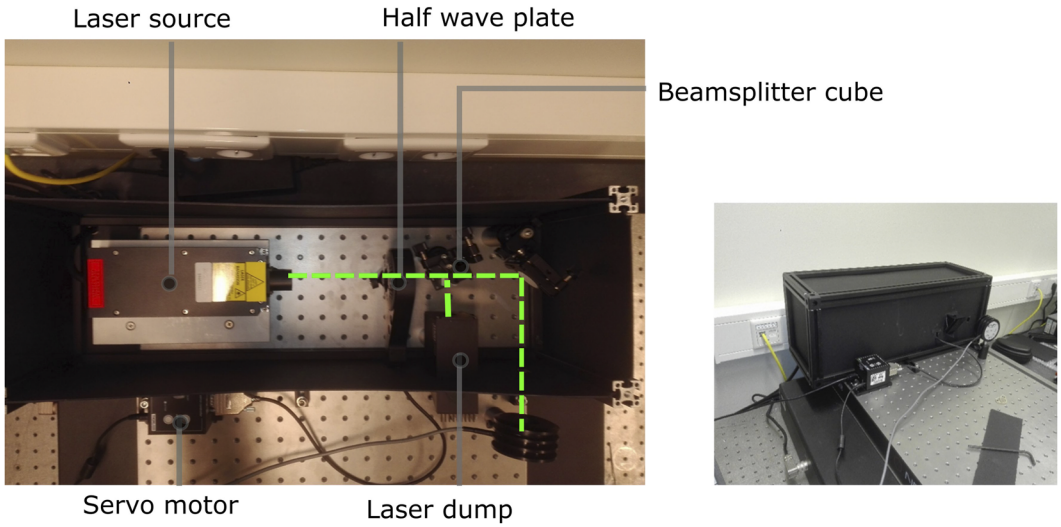

FIG. 3. Laser power control: the laser source emits at 1 W constant. The laser light (light green in the image) passes through a rotational stage with a half wave plate mounted. The beamsplitter cube deflects part of the laser power to a dump, while the rest passes through and exits the box. All components are enclosed in a box for safety reasons.

(Thorlabs LPVISE100-A) is placed on a rotational stage (Thorlabs CLR1/M) followed by an achromatic fixed magnification beam expander (Thorlabs GBE15-A) and finally the camera. The camera, a Fastec HiSpec 1 CMOS sensor with 506 fps at the resolution of 1280 × 1024 pixels and 113 000 fps at 128 × 2 pixels, 14 × 14 μm^2 pixel size, and an internal memory of 4 GB, is controlled by dedicated software (HiSpec Control Software). These optical components allows a field of view of about 800 × 700 μm^2 using all available pixels or a 50 × 50 μm^2 field of view using 100 × 100 pixels when the camera speeds up to 20 000 fps.

III. LSI

In the printing of ink, the time required for drying of a droplet plays a fundamental role in printing features. If the ink dries too fast or too slow, the subsequently printed droplet may not fuse properly with the previous droplet, creating artifacts in the final product.[37,38] Modern printheads print thousands of picoliter droplets every second. There are a number of interactions that occurs when a droplet hits a substrate: first, the ink wets the surface, followed by spreading and absorption, together with evaporation. These events concur in the drying process. The time required for a single droplet to complete its drying process is usually from fraction of second to seconds, depending on the ink composition and the substrate, which may also swell. In addition, the request from the industry for higher printing speed and quality requires a deeper understanding of the dynamics that occur at these short timescales. Given the micrometric dimension and the high drying speed, the above described High-Speed Laser Speckle Imaging (HS-LSI) technique fits well by adapting the current understanding of the LSI technique to higher speeds up to 20 000 fps, meaning one acquisition every $5 \cdot 10^{-5}$ s. By employing HS-LSI and printing drops-on-demand by jetting multiple 10 pl volume drops, the fast dynamics of the interaction beneath and in proximity of the drop at the nanometer length scale are resolved.

If a droplet is printed in the field of view, immediately after a polarized laser beam illuminates the sample, the photons of the beam scatter off of the sample, from both the contents of the ink and the underlying substrate. The emerging scattered light passes through a series of optical components, magnifying the speckle pattern and selecting only multiply scattered photons using an analyzer, thus avoiding single scattered photons. This is done by rotating the analyzer until the light intensity that reaches the camera sensor is minimized: indeed, we measure a considerable amount of light arising from surface reflection. To have a good HS-LSI measurement, only photons that have scattered enough times to be in the multiscattered regime are collected by the camera and may be treated as having performed a random walk.[32,39,40] This requirement ensures that the emerging photons lose their directionality and phase, therefore exhibiting constructive and destructive interference, and that on the camera detector will appear as a speckle pattern, as shown in Fig. 4. If there is motion within the sample arising within the ink or substrate, the photons experience different scattering events and therefore different path lengths result in a speckle pattern that fluctuates in time. For each time step, for instance, 10^{-4} s at 10 000 fps, a raw speckle image is collected by the camera. Any individual image contains a map of gray values ranging from 0 to 255 for the 8-bit camera CCD that indicate the light intensity; to avoid artifacts in the analysis adjustment, both laser power and camera shutter time are adjusted such that the most intensity values fall within the correct range, eliminating over- and sub-exposed images.

Two main methods are utilized to analyze the saved images: autocorrelation functions, namely, $g_2(\tau)$ and $d_2(\tau)$, and the Fast Fourier transform (FFT) analysis.[41] Autocorrelation functions have been widely used to exploit different scenarios, such as liquid imbibement and crack healing,[19,42] as well as for routine measurements, such as DLS. Previous works involving these functions can be found in publications from this journal[43] or elsewhere.[44,45] The correlation functions, $g_2(\tau)$ and $d_2(\tau)$, are related to the amount of motion of the scatterers, mostly titania nanoparticles in the present case. From these mobilities, the physical quantities that can be defined are the radius of the imbibed region, the mean squared displacement, and their evolution with time. This time dependence reveals for each time step if we are observing super- or subdiffusional processes or the speed of the moving drying or wetting front of the jetted picoliter droplets. We can measure both these functions with high spatial and temporal precision using HS-LSI. It has also been proven in previous works that quantities such as mean squared displacement, viscosity, and free energy can be evaluated from the $g_2(\tau)$ and $d_2(\tau)$ autocorrelation functions.[25] Depending on the system under consideration, one or both of these functions can be more useful to describe the ongoing process. We found that in most of the cases, the $d_2(\tau)$ function is more sensitive to small-scale displacement than the $g_2(\tau)$ function, as reported in Ref. 46; this is due to the difference nature of $d_2(\tau)$ in contrast to the multiplicative form of $g_2(\tau)$.

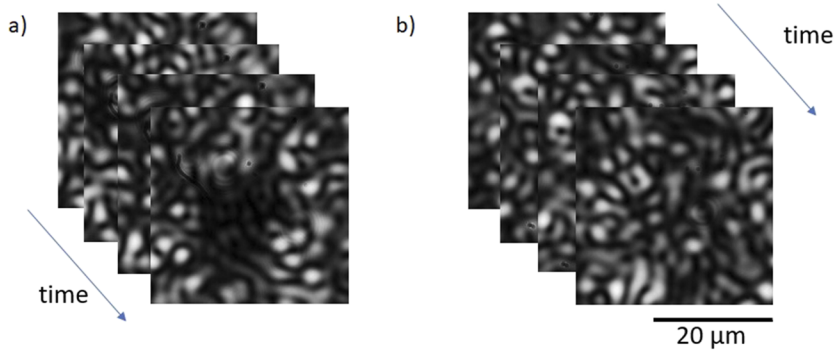

FIG. 4. Raw speckle images for (a) black ink and (b) titania ink. Black bar represent 20 μm.

The explicit form for the two quantities can be read as follows:

$$g_2(t,x,y,\tau) = \frac{\langle I(t,x,y)\cdot I(t+\tau,x,y)\rangle}{\langle I(t,x,y)\rangle\langle I(t+\tau,x,y)\rangle},$$
$$d_2(t,x,y,\tau) = \frac{\langle [I(t,x,y) - I(t+\tau,x,y)]^2\rangle}{\langle I(t,x,y)\rangle\langle I(t+\tau,x,y)\rangle}, \quad (1)$$

where τ represents the sampled correlation time, acting as a tuning knob for creating image contrast. The range of dynamics that can be explored with this method are wide: the lower bound resolution is given by the frame rate, while the upper bound is given by the total measurement time, limited by the internal memory storage of the camera. Note that differently from DWS, where only a single speckle per time is analyzed, in LSI, in order to increase the statistics, spatial averaging occurs within a ROI. It is possible to fit the g_2 function, making use of the Siegert relation, to a single-exponential decay to calculate the normalized field autocorrelation function, namely, $g_1(t, \tau)$,

$$g_1(t,\tau) = \frac{1}{\sqrt{\beta}}\sqrt{g_2(t,\tau)-1} = \exp[-\gamma[\tau/\tau_0(t)]^{\alpha(t)}], \quad (2)$$

where α is the stretching exponent and yields information on the nature of sample dynamics on the spatial length scale of the ROI: subdiffusive for $\alpha < 0.5$, diffusive for $\alpha = 0.5$, and superdiffusive for $\alpha > 0.5$. Addition to this stretching exponent, $\tau_0(t)$ is the time evolution of a characteristic time scale, τ_0. The key disadvantage of the $g_2(\tau)$ analysis, even though having been extensively used in a variety of scenarios,[24,28,42,47] is the computational time required. Depending on the ROI utilized and the total number of frames, the computational time can vary from hours to a full day.

A recent development in LSI analysis has shown that using a Fast Fourier transform (FFT) approach can be orders of magnitude faster than $g_2(\tau)$ analysis.[41] Using this approach, the analysis moves from the time domain to the frequency domain, resulting in a power spectra density to quantify the speckle fluctuation in the frequency domain. The FFT analysis is performed for a series of N images, which means to act on a time series of speckle images. For each pixel of the time series at first, the average of all the series is subtracted in order to have the intensity fluctuation around a mean of zero. A standard FFT routine allows moving from the time domain to the frequency domain,[48] and the power spectrum is obtained by computing the single-sided spectrum, squaring the result and normalizing it dividing by $(\langle I^2\rangle - \langle I\rangle^2)$. Note that with this approach, spatial information is lost. However, the Wiener–Kinchin theorem ensures that the autocorrelation function and the power spectral density contain the same quantitative information, but this approach is computationally much faster than the g_1 correlation.

IV. HIGH-SPEED LSI

A. Materials

To test the instrument, we used two different substrates: glass filters (Duran™ sintered glass filter disc, 25 mm diameter, pore size 1–1.6 μm) and Teslin paper. The former material has been chosen as it is unable to swell while the pore size and surface properties mimic common printing paper. A substrate with no swelling ensures that the recorded dynamics are associated only with the movement of the particles composed of the tested ink. Indeed, LSI can only be applied to moving scattering objects. In the absence of motion, the speckle pattern does not exhibit any fluctuations: only moving particles and/or moving fibers are able to change the photons path; otherwise, the result is a static speckle image. Additionally, the nominal pore size of these filter disks is comparable to the one of the common printing paper mimicking its permeability. The second material tested, Teslin paper, is a waterproof synthetic printing medium manufactured by PPG Industries. Teslin is a single-layer, uncoated film, which is mechanically extremely strong, 2–4 times stronger than other coated synthetic and coated papers, while being recyclable and non-toxic. This kind of paper is commonly used by printing companies to test new ink formulations.

Three inks are used: two commercial inks, containing black and magenta pigments with a latex binder, which exhibit a similar behavior, and a home-made ink, prepared with MilliQ water, glycerol, surfactant (Triton X-100, Sigma-Aldrich), and titania particles (titanium oxide nanopowder, 30 nm particle size, acquired from US Research Nanomaterials). We observe that black and magenta inks absorb most of the incoming laser light, while titania particles are highly reflective, resulting in a higher intensity of collected signal. Additionally, the number of scattering events for the titania ink is higher with respect to the commercial inks, ensuring scattered photons to be in the multiple scattering regime—a crucial requirement to perform accurate LSI measurements. To work with commercial ink, titania particles are added by sonication, which resulted in an increased opacity, allowing for LSI measurements.

Measurements were performed on the inks to evaluate their macroscopic general properties. Contact angle measurements (Kruss Drop Shape Analyzer—DSA100, used with a custom-made software) were performed on macroscopic drops, of ~0.05 ml each, at room temperature; this volume being 4 orders of magnitude larger than the printed picoliter drop, as such it is expected to behave differently. The contact angle measurement was made manually by selecting the drop boundary, on the collected drop shape images, to fit it into a parabolic shape. In addition to the glass filter and Teslin paper, a third substrate of a cleaned solid glass slide (Thermo Scientific microscope glass slide) was used to test the inks. Results for the different compositions are shown in Table I. Commercial inks exhibit a lower value of contact angle, demonstrating their tendency to spread and wet more than the titania ink. The same observation can be applied comparing the three substrates. The wetability of the Teslin paper is lower than the filter disks and glass slides for all cases. Rheological measurements of viscosity were performed on the three inks showing Newtonian behavior. The viscosity values for the titania ink is (0.0187 ± 0.0008) Pa s, which is higher with respect to

TABLE I. Contact angle right after the drop deposition.

Ink	Glass	Filter disk	Teslin paper
Black	40	52	53
Magenta	37	50	54
Titania	44	67	>90
Water	19.5	29	>90

the value of (0.0062 ± 0.0003) Pa s found for commercial inks. The higher value for the titania reflects the fact that the picoliter drops produced with this ink have approximately double the volume with respect to commercial inks.

B. Application

HS-LSI can be used to unravel the behavior of picoliter droplets for the considered inks on commercial Teslin paper. After having loaded the cartridge with the desired ink, the MATLAB GUI starts the printhead to move on the rail, and when it reaches the movement sensor, a series of droplets are printed on the desired location, illuminated hereafter by the laser. After having experienced the sample, part of the outcoming light is directed toward the optics and therefore to the camera sensor: raw speckle images are acquired. One example of raw speckle image acquisition at 10 000 fps for both black and titania picoliter drop inks is shown in Fig. 4. To be able to reach these values in the frame rate and to keep a duty cycle of the camera under the limit of 100%, an exposure time of less than 100 μs is required. If the exposure time is shortened, an increased laser light is needed to have gray levels distributed over full bit-depth of the captured image. The direct consequence of an increased laser power is an increment of the temperature at the location of the laser spot, thus resulting in a thermal effect that has to be avoided in these preliminary stages. Local laser exposure does result in an enhanced thermal diffusive effect not associated with drying, and we have experimentally minimized this effect in these preliminary experiments. To quantify this effect, an infrared sensor, PCE-IR 51, was mounted to check the variation of temperature on the sample. The substrate temperature, considering the laser power we used in these measurements, does not exceed 35 °C. To have a consistent set of measures, we have maintained an almost identical laser power for all the droplets during all measurements. A cooling component, for example, a Peltier element, could have been implemented to maintain a constant temperature of the substrate, but the ink surface would still be dominated by the laser heating effect. Thus, we directed our attention to maintaining a constant laser power and thus a nearly constant local heating of the droplets, allowing for qualitative comparisons between droplets. A reasonable cutoff to avoid this thermal effect in the case of titania ink and Teslin paper is using a limited sampling frequency of 2 kHz, with an exposure time of 500 μs per frame. Since printing the drop within micrometric precision is challenging, the camera ROI is set to have a size of ~200 × 150 μm^2. Using these parameters, the total experimental time is limited by the physical memory of the camera, which is in the order of tens of seconds. A bigger ROI would imply a shorter total experimental time but necessitate a lower positional accuracy of the printed droplet.

One example showing the time evolution of a picoliter drop from an acute angle not normal to the droplet observed using white light is presented in Fig. 5(a) (Multimedia view). These images were collected to provide a visual interpretation of the overall printing process. We note that approximately after 5–6 s, depending on the volume of the ejected drop, which is not precisely controlled, the ink is completely imbibed into the substrate. This auxiliary camera from a side view allows us to collect the relative volume of the drop above the substrate, allowing for the drop volume evolution with time.

Scattered light from a similar drop is observed from the normal direction and analyzed using the LSI d_2 correlation function, as shown in Fig. 5(b) (Multimedia view). In most cases, an enhanced mobility is seen during the first second after the deposition. Afterward, there is a decreased mobility during the following 5 s, in which imbibition and the evaporation process take place.

Interestingly, under certain conditions, which require deeper investigation, some of the drops exhibit increased mobility at the moment just before complete imbibition; this feature cannot be observed using white light illumination and thus must be microscopic in nature. This mobility is likely associated with a rush hour effect: a fast rearrangement of scattering titania particles and/or paper fibers when the water is nearly completely absent. As pointed out in Refs. 25 and 49, this effect can be present and concomitant with the pinning of the contact line, since evaporation here is rapid than that of the bulk of the droplet. Yet, in our case, we expect the surface of the substrate, considering the micrometric droplet size, to behave differently from a macroscopic droplet. SEM images acquired after the drying of the droplet show contrasting drying patterns from the model proposed for millimeter-sized droplets, making comparison between the two length scales an ongoing yet intriguing challenge. For instance, micrometer scale droplets, as used in this work, are of similar dimension to the typical roughness of substrates, such as paper, and thus, the pinning of the contact line by paper fibers is expected to play a more significant role. This kind of event is not observed in the cases of glass disk substrates, so we suspect that the rearrangement of the particles in contact with the paper fibers of the Teslin substrate increases in mobility. We choose to give this interpretation because we are able to monitor the size of the liquid cap which remains outside of the substrate; in the presented case, the increased motion takes place on a region which is approximately the same size of all the imbibed region, implying that the motion we record is not given only from the liquid cap but mostly from the dispersed titania particles on and in the substrate. However, it is possible that the recorded motion is caused from the presence and the final drying of a lubricant film on top of the substrate, as numerically and experimentally exposed from Refs. 50 and 51. One final possibility to explain this observation could be the presence of multiple depinning events. As previously stated, we believe this effect needs deeper investigation. We must emphasize again that the aim of this paper is not only the interpretation of the data obtained but also the novelty and the possibilities this instrumentation can yield toward these unresolved phenomena. Thus, we limited the analysis of the resulting data to only a qualitative level. The exposition of a mathematical model and its interpretation will be exposed in a subsequent work. Previous works utilizing LSI[25,52] have shown, however, that it is possible to obtain quantities that can be implemented in mathematical models. We believe that understanding the physics/chemistry that happens on a micrometer scale can give us the possibility to obtain significant advances also in the understanding of millimeter scale droplet behavior by combining these experimental results with the existing models of droplet drying.[49–51]

Such a description remains qualitative, and to obtain a more complete overview over the entire process, we can benefit from FFT and g_2 analysis, as presented, respectively, in Figs. 5(c) and 5(d). These results are obtained analyzing the same drop of titania ink on Teslin paper.

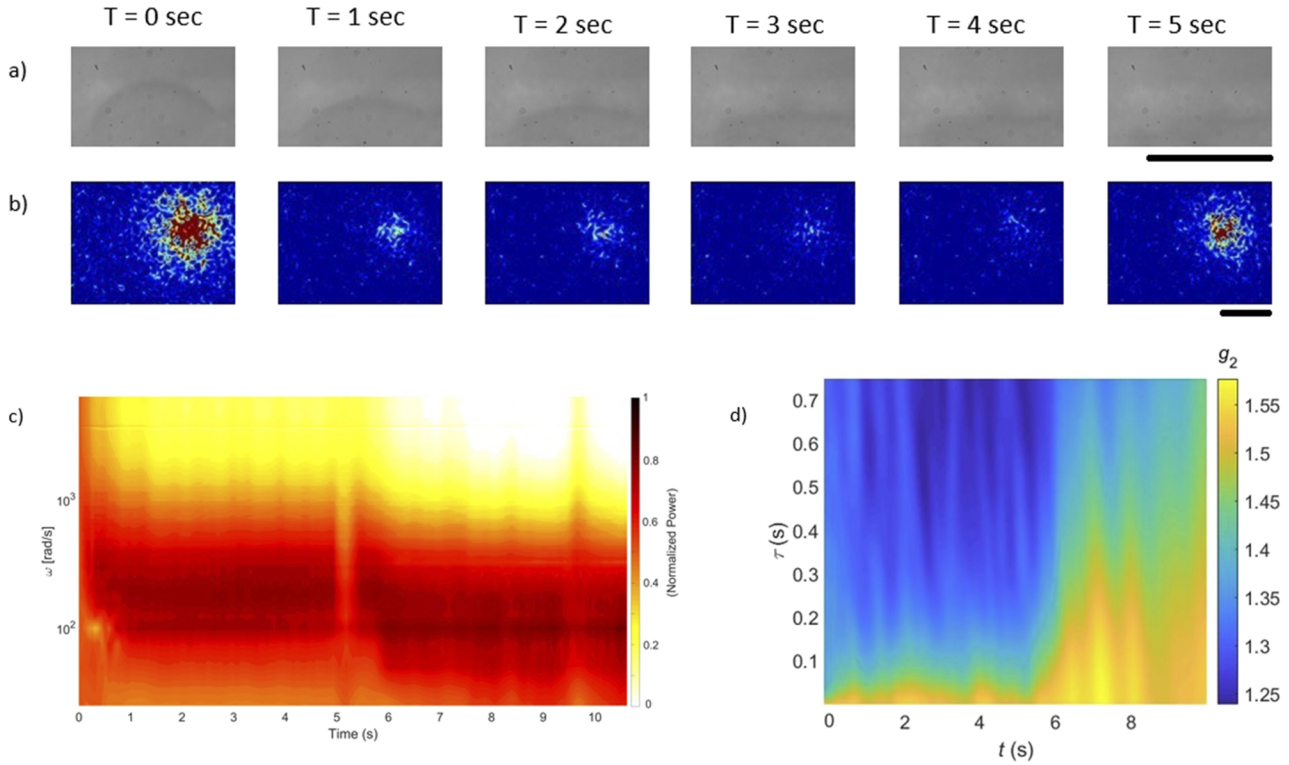

FIG. 5. Time evolution of a picoliter titania ink drop on Teslin paper. (a) Side view of the drop evolution under white light exposure. On average, after 5–6 s, we observe that the drop is completely imbibed into the substrate. Black scale bar represents 25 μm. A video is included with a field of view of ~30 × 25 μm^2, shown at 10 fps with a total length of 8 s. (b) d_2 analysis of the evolution from top view was performed with a step of 200 frames, resulting in one d_2 image every 0.1 s. Red pixels indicate higher mobility. Black scale bar represents 25 μm. A video is included with a field of view of ~80 × 60 μm^2 captured at 2000 fps, shown at 10 fps with a total length of 8 s. (c) Spectrograms resulting from the FFT routine and (d) g_2 analysis obtained from the same drop. Mutimedia views: (a) https://doi.org/10.1063/5.0011167.1 and (b) https://doi.org/10.1063/5.0011167.2

An FFT routine, developed as reported in Ref. 41, results in a spectrogram, shown in Fig. 5(c); on the x axis, the experiment time is expressed in seconds, while on the y axis, the frequencies are expressed in radiant per second, obtained from the deconvolution of the variation in pixel intensity of the HS-LSI speckle time series images. We observe an enhancement of all frequencies for the first half second, immediately after the drop hits the substrate and the first interaction with the paper occurs. This initial process is followed by a reduction in relative intensities for higher frequencies at first, and after 1 s, also at lower frequencies. A change in the resulting spectrogram occurs after 5.5/6 s when the drop is completely imbibed from the substrate. Frequencies above 10^3 Hz are now absent, meaning a slow-down of the droplet dynamics. Lower frequencies, and thus slower dynamics, associated with the motion of the liquid inside the substrate remain present for the rest of the experimental time. Using the same ink and substrate, we can increase the total experimental time at the cost of the frame rate. Operating at 500 fps, we can detect motions even after 40 s; these dynamics are clearly not visible with other techniques. We suspect that the smaller spikes observed in this spectrogram are generated by variations in laser intensities that occur at the time scale of the microsecond. The same features and interpretation can be deduced from Fig. 5(d), where we made use of the g_2 analysis as in Ref. 47. Also here the experimental time is displayed on the x axis, while on the y axis, the correlation time is expressed in seconds. For each fixed experimental time, we vary the correlation time τ expressed in Eq. (1) to finally obtain a g_2 correlation curve. Higher g_2 values indicate lower mobility for the considered correlation time. It is possible to observe in both approaches, FFT and g_2, an abrupt increase in mobility at 5 s, associated with the fast rearrangement of the materials when droplet imbibement is over, represented as an increase in activity in mid-frequencies in the case of the FFT, or as a lower value, represented as disappearance of blue g_2 values in Fig. 5(d). The remarkable advantage of using the FFT approach is the net decrease in computational time, from tens of hours for g_2 routine to minutes with FFT routine, required to analyze the raw speckle images.

V. CONCLUSIONS

We present in this article a new generation of LSI instrumentation: a new tool that has the ability to unravel dynamics that happen at the time scale of a single millisecond and the length scale of a single nanometer. This instrument is capable of printing-on-demand

picoliter volume drops of ink, both commercial and self-produced, on different substrates utilizing a moving printing cartridge while moving at a speed of 1 m/s with printing positional precision of tens of micrometer. We have described in detail how the instrument is designed to overcome challenges unique to LSI, in particular, vibration sensitivity. We have also described the basics of the LSI technique and how it can be adapted to be sensitive to the fast rearrangement of particles that comprise the ink and the scattering substrate reaching a sampling frequency of 20 kHz. Finally, we gave one example of its usage and showed its power in unraveling some features that cannot be observed using other techniques, allowing for a more complete description of wetting and imbibition processes of ink on the porous substrate. A complete physio-chemical description of the printing, imbibement, and swelling processes associated with commercial inkjet printing are currently under investigation using this HS-LSI instrument.

SUPPLEMENTARY MATERIAL

The supplementary material contains a detailed description of the supporting movies of high-speed laser speckle imaging.

AUTHORS' CONTRIBUTIONS

All authors contributed equally to this work.

ACKNOWLEDGMENTS

T. E. Kodger acknowledges funding from the Dutch Science Organization (NWO) through the Veni funding scheme and J. Sprakel acknowledges funding from NWO through the Vidi funding scheme. The collaboration and support received from the Canon Production Printing company are acknowledged.

DATA AVAILABILITY

The data that support the findings of this study are available from the corresponding author upon reasonable request.

REFERENCES

[1]K. Sefiane, "Patterns from drying drops," Adv. Colloid Interface Sci. **206**, 372–381 (2014).
[2]S. El-Molla, "Inkjet printing & spray deposition techniques for flexible electronic applications," Doctoral dissertation, Technische Universität München, 2017.
[3]H. Aslannejad, H. Fathi, S. M. Hassanizadeh, A. Raoof, and N. Tomozeiu, "Movement of a liquid droplet within a fibrous layer: Direct pore-scale modeling and experimental observations," Chem. Eng. Sci. **191**, 78–86 (2018).
[4]S. Wiryana and J. C. Berg, "The transport of water in wet-formed networks of cellulose fibers and powdered superabsorbent," Wood Fiber Sci. **23**, 457–464 (1991).
[5]S. Sousa, J. A. Gamelas, A. de Oliveira Mendes, P. T. Fiadeiro, and A. Ramos, "Interactions of ink colourants with chemically modified paper surfaces concerning inkjet print improvement," Mater. Chem. Phys. **139**, 877–884 (2013).
[6]V. M. Starov, S. A. Zhdanov, S. R. Kosvintsev, V. D. Sobolev, and M. G. Velarde, "Spreading of liquid drops over porous substrates," Adv. Colloid Interface Sci. **104**, 123–158 (2003).
[7]V. M. Starov, S. R. Kosvintsev, V. D. Sobolev, M. G. Velarde, and S. A. Zhdanov, "Spreading of liquid drops over saturated porous layers," J. Colloid Interface Sci. **246**, 372–379 (2002).
[8]C. Van Roost and G. Desie, "Validation of ink media interaction mechanisms for dye and pigment-based aqueous and solvent inks," J. Imaging Sci. Technol. **50**, 294–303 (2006).
[9]S. B. Siegel, "Ink jet UV curing," U.S. patent 7,137,696 (21 November 2006).
[10]J. Segurola, N. S. Allen, M. Edge, and A. Mc Mahon, "Design of eutectic photoinitiator blends for UV/visible curable acrylated printing inks and coatings," Prog. Org. Coat. **37**, 23–37 (1999).
[11]Y. Yang and S. Li, "Cotton fabric inkjet printing with acid dyes," Text. Res. J. **73**, 809–814 (2003).
[12]T. Sweijen, E. Nikooee, S. M. Hassanizadeh, and B. Chareyre, "The effects of swelling and porosity change on capillarity: DEM coupled with a pore-unit assembly method," Transp. Porous Media **113**, 207–226 (2016).
[13]D. R. Schuchard and J. C. Berg, "Liquid transport in composite cellulose—Superabsorbent fiber networks," Wood Fiber Sci. **23**, 342–357 (2007).
[14]C. Diddens, "Detailed finite element method modeling of evaporating multi-component droplets," J. Comput. Phys. **340**, 670–687 (2017).
[15]V. Joekar-Niasar and S. M. Hassanizadeh, "Analysis of fundamentals of two-phase flow in porous media using dynamic pore-network models: A review," Crit. Rev. Environ. Sci. Technol. **42**, 1895–1976 (2012).
[16]X. Yin, H. Aslannejad, E. T. de Vries, A. Raoof, and S. M. Hassanizadeh, "Droplet imbibition into paper coating layer: Pore-network modeling simulation," Transp. Porous Media **125**, 239–258 (2018).
[17]H. Tan, C. Diddens, P. Lv, J. G. M. Kuerten, X. Zhang, and D. Lohse, "Evaporation-triggered microdroplet nucleation and the four life phases of an evaporating Ouzo drop," Proc. Natl. Acad. Sci. U. S. A. **113**, 8642–8647 (2016).
[18]J. D. Briers, "Laser Doppler, speckle and related techniques for blood perfusion mapping and imaging," Physiol. Meas. **22**, R35 (2001).
[19]H. M. van der Kooij, G. T. van de Kerkhof, and J. Sprakel, "A mechanistic view of drying suspension droplets," Soft Matter **12**, 2858–2867 (2016).
[20]D. Briers, D. D. Duncan, E. R. Hirst, S. J. Kirkpatrick, M. Larsson, W. Steenbergen, T. Stromberg, and O. B. Thompson, "Laser speckle contrast imaging: Theoretical and practical limitations," J. Biomed. Opt. **18**, 066018 (2013).
[21]B. Weber, C. Burger, M. T. Wyss, G. K. von Schulthess, F. Scheffold, and A. Buck, "Optical imaging of the spatiotemporal dynamics of cerebral blood flow and oxidative metabolism in the rat barrel cortex," Eur. J. Neurosci. **20**, 2664–2670 (2004).
[22]A. K. Dunn, H. Bolay, M. A. Moskowitz, and D. A. Boas, "Dynamic imaging of cerebral blood flow using laser speckle," J. Cereb. Blood Flow Metab. **21**, 195–201 (2001).
[23]D. J. Pine, D. A. Weitz, P. M. Chaikin, and E. Herbolzheimer, "Diffusing wave spectroscopy," Phys. Rev. Lett. **60**, 1134 (1988).
[24]A. Amon, A. Mikhailovskaya, and J. Crassous, "Spatially resolved measurements of micro-deformations in granular materials using diffusing wave spectroscopy," Rev. Sci. Instrum. **88**, 051804 (2017).
[25]H. M. van der Kooij, S. Dussi, G. T. van de Kerkhof, R. A. M. Frijns, J. van der Gucht, and J. Sprakel, "Laser speckle strain imaging reveals the origin of delayed fracture in a soft solid," Sci. Adv. **4**, eaar1926 (2018).
[26]H. M. van der Kooij, S. A. Semerdzhiev, J. Buijs, D. J. Broer, D. Liu, and J. Sprakel, "Morphing of liquid crystal surfaces by emergent collectivity," Nat. Commun. **10**, 3501 (2019).
[27]S. A. Semerdzhiev, H. M. van der Kooij, R. Fokkink, and J. Sprakel, "Rapid and unambiguous determination of the open time for waterborne paint films with laser speckle imaging," arXiv:1903.09691 (2019).
[28]H. M. van der Kooij, R. Fokkink, J. van der Gucht, and J. Sprakel, "Quantitative imaging of heterogeneous dynamics in drying and aging paints," Sci. Rep. **6**, 34383 (2016).
[29]L. Baij, J. Buijs, J. J. Hermans, L. Raven, P. D. Iedema, K. Keune, and J. Sprakel, "Quantifying solvent action in oil paint using portable laser speckle imaging," Sci. Rep. **10**, 10574 (2020).
[30]L. Vitomir, J. Sprakel, and J. van der Gucht, "Spatial blurring in laser speckle imaging in inhomogeneous turbid media," Sci. Rep. **7**, 16879 (2017).

[31] D. A. Weitz, J. X. Zhu, D. J. Durian, H. Gang, and D. J. Pine, "Diffusing-wave spectroscopy: The technique and some applications," Phys. Scr. **T49B**, 610 (1993).
[32] R. Lenke and G. Maret, *Multiple Scattering of Light: Coherent Backscattering and Transmission* (Gordon and Breach, Amsterdam, The Netherlands, 2000), pp. 1–73.
[33] M. Bahoura and M. A. Noginov, "Determination of the transport mean free path in a solid-state random laser," J. Opt. Soc. Am. B **20**, 2389–2394 (2003).
[34] P.-E. Wolf and G. Maret, "Weak localization and coherent backscattering of photons in disordered media," Phys. Rev. Lett. **55**, 2696 (1985).
[35] K. Busch, C. M. Soukoulis, and E. N. Economou, "Transport and scattering mean free paths of classical waves," Phys. Rev. B **50**, 93 (1994).
[36] L. F. Rojas-Ochoa, D. Lacoste, R. Lenke, P. Schurtenberger, and F. Scheffold, "Depolarization of backscattered linearly polarized light," J. Opt. Soc. Am. A **21**, 1799–1804 (2004).
[37] J. Stringer and B. Derby, "Formation and stability of lines produced by inkjet printing," Langmuir **26**, 10365–10372 (2010).
[38] N. Jones, S. J. Sargeant, K. Sargeant, J. C. Briggs, and M.-K. Tse, "Characterizing and modeling coalescence in inkjet printing," in *NIP and Digital Fabrication Conference* (Society for Imaging Science and Technology, 1998), Vol. 1, pp. 161–166.
[39] D. J. Pine, D. A. Weitz, J. X. Zhu, and E. Herbolzheimer, "Diffusing-wave spectroscopy: Dynamic light scattering in the multiple scattering limit," J. Phys. **51**, 2101–2127 (1990).
[40] F. C. MacKintosh and S. John, "Diffusing-wave spectroscopy and multiple scattering of light in correlated random media," Phys. Rev. B **40**, 2383 (1989).
[41] J. Buijs, J. van der Gucht, and J. Sprakel, "Fourier transforms for fast and quantitative laser speckle imaging," Sci. Rep. **9**, 13279 (2019).
[42] H. M. van der Kooij, A. Susa, S. J. García, S. van der Zwaag, and J. Sprakel, "Imaging the molecular motions of autonomous repair in a self-healing polymer," Adv. Mater. **29**, 1701017 (2017).
[43] A. P. Y. Wong and P. Wiltzius, "Dynamic light scattering with a CCD camera," Rev. Sci. Instrum. **64**, 2547–2549 (1993).
[44] J. Wagner, W. Härtl, and R. Hempelmann, "Characterization of monodisperse colloidal particles: Comparison between SAXS and DLS," Langmuir **16**, 4080–4085 (2000).
[45] G. Maret and P. E. Wolf, "Multiple light scattering from disordered media. The effect of Brownian motion of scatterers," Z. Phys. B: Condens. Matter **65**, 409–413 (1987).
[46] K. Schätzel, "Correlation techniques in dynamic light scattering," Appl. Phys. B: Photophys. Laser Chem. **42**, 193–213 (1987).
[47] H. M. van der Kooij, M. de Kool, J. van der Gucht, and J. Sprakel, "Coalescence, cracking, and crack healing in drying dispersion droplets," Langmuir **31**, 4419–4428 (2015).
[48] G. D. Bergland, "A guided tour of the fast Fourier transform," IEEE Spectrum **6**, 41–52 (1969).
[49] L. Espín and S. Kumar, "Droplet spreading and absorption on rough, permeable substrates," J. Fluid Mech. **784**, 465 (2015).
[50] T. Pham and S. Kumar, "Drying of droplets of colloidal suspensions on rough substrates," Langmuir **33**, 10061–10076 (2017).
[51] T. Pham and S. Kumar, "Imbibition and evaporation of droplets of colloidal suspensions on permeable substrates," Phys. Rev. Fluids **4**, 034004 (2019).
[52] P. Zakharov, A. Völker, A. Buck, B. Weber, and F. Scheffold, "Quantitative modeling of laser speckle imaging," Opt. Lett. **31**, 3465–3467 (2006).